

Improving Bone Graft Incorporation Through Sustained, Local Delivery of FTY720

---

A Thesis  
Presented to  
the faculty of the School of Engineering and Applied Science  
University of Virginia

---

in partial fulfillment  
of the requirements for the degree  
Master of Science

by

Cynthia Sarah Huang

December  
2012

APPROVAL SHEET

The thesis  
is submitted in partial fulfillment of the  
requirements for the degree of  
Master of Science

  
AUTHOR

The thesis has been read and approved by the examining Committee:

Edward Botchwey

---

Advisor

Kimberly Kelly

---

Quanjun Cui

---

Accepted for the School of Engineering and Applied Science:

  
Dean, School of Engineering and Applied Science

December  
2012

## **Abstract**

Massive bone allografts commonly used for craniofacial reconstruction can exhibit challenging complications such as non-union, fracture, or rejection. Growing evidence suggests the largest barrier to successful long term allograft incorporation is delayed or absent vascularization, as bone grafts are difficult to vascularize. To this end, this work utilized two novel bone graft drug loading strategies to sustain the local release of FTY720, a selective agonist for sphingosine 1-phosphate (S1P) receptors, in rat cranial defects: loaded in a coating of poly(lactic-co-glycolic acid) (PLAGA) or directly adsorbed to graft. To explore the polymer coating delivery method, uncoated grafts, vehicle coated, low dose FTY720 in PLAGA (1:200 w:w) and high dose FTY720 in PLAGA (1:40) were implanted into critical size calvarial bone defects. The ability of local FTY720 delivery to promote angiogenesis, maximize osteoinductivity, and improve graft incorporation by recruitment of bone progenitor cells from surrounding soft tissues and microcirculation was evaluated. FTY720 bioactivity after polymer encapsulation and release was confirmed with a sphingosine kinase 2 assays. HPLC-MS quantified about 50% loaded FTY720 release of total encapsulated drug (4.5 µg) after 5 days. Following 2 weeks of defect healing, FTY720 delivery led to statistically significant increases in bone volumes compared to controls. The rate and extent of enhanced bone growth persisted through week 4, but by week 8, increases in bone formation in FTY720 groups were no longer statistically significant. However, micro-computed tomography (microCT) of contrast enhanced vascular ingrowth (MICROFIL®) and histological analysis showed enhanced integration as well as directed bone growth in both high and low dose FTY720 groups compared to controls.

The cranial defect model was again used to explore direct adsorption of FTY720 to bone grafts as a therapy with empty defects, xenograft only, or FTY720 loaded xenografts. Again, FTY720 improved graft remodeling and enhanced bone healing in the void space starting after week 2 and continuing through week 12. Empty defects saw undirected bone growth which began to regress after week 10. This work capitalized on existing mechanical and biomaterial properties of devitalized bone and delivered a small molecule compound to constitutively target vascular and osseous remodeling at the graft-host bone interface. Such results support continued evaluation of drug-eluting grafts as a viable strategy to improve functional outcome and long-term success of massive bone graft implants.

## **Acknowledgements**

This work was only possible with the support of many people, institutions, and funding sources. Thank you, all.

First and foremost, Dr. Edward Botchwey, my advisor, who was willing to give me a chance from day one. You continually supported my growth as a researcher by providing unparalleled mentoring and perspective. I admire you most highly and will always be grateful for everything you have done. I count myself extremely lucky to have been your graduate student for even a minute, much less over three years.

My thesis committee consisting of Dr. Kimberly Kelly and Dr. Quanjun Cui, who have given crucial, experienced insight and guidance.

Dr. Roy Ogle, for being the most motivating and supportive mentor that I could wish for. Becca Ogle, for significant research help.

Dr. Kevin Lynch, for his lively discussions and vital collaboration. His lab members Jose Tlaxa, Yugesh Kharel, Perry Kennedy, and Amanda Gillett also provided crucial research aid and experience.

Fellow UVA BMEs for teaching invaluable techniques, lending time or items, and providing a wonderful environment for research. Particularly Anthony Bruce, Liz Logsdon, Josh Meisner, Bryan Piras, Mark Seaman, Ji Song, and Stephanie Thomas.

All of my professors, especially Dr. Brian Duling, Dr. Brian Helmke, Dr. Jeffery Holmes, Dr. Jason Papin, and Dr. Shayn Peirce-Cottler, whose classroom instruction helped elevate my education to improve my cognitive abilities and research work.

My fellow UVA graduate students and friends who were with me through every success, failure, and times of hard work and fun in between.

All my Botchwey lab mates, particularly: Anthony Awojoodu, Carol Bampoe, Dr. Dan Barker, Dan Bowers, Brittany Bullock, Nathan Chiappa, Dr. Anusuya Das, Molly Dickinson, Lana Hoang, Dr. Brian Hughley, Silvia LaRue, Steven Lenz, Yong Lin, Parker Merrill, Dr. Rebekah Neal, Ethan Nyberg, Dr. Molly Ogle, Tyler Pegoraro, Claire Segar, Soo Shin, Michael Tanes, Dr. Shaun Tanner, Dr. Sunil Tholpady, Tiffany Wang, and Matt Williams, whose support, discussion, and assistance

My supportive, loving, and reliable family.

## Table of Contents

APPROVAL SHEET .....	ii
ABSTRACT.....	iii
ACKNOWLEDGEMENTS.....	v
TABLE OF CONTENTS.....	vi
LIST OF TABLES AND FIGURES.....	vii
LIST OF SYMBOLS/ABBREVIATIONS.....	viii
INTRODUCTION.....	1
METHODS.....	5
RESULTS.....	16
DISCUSSION.....	33
CONCLUSION.....	38
REFERENCES.....	39

## List of Tables and Figures

Figure 1.	Rat subperiosteal and cranial defect models. . . . .	3
Table 1.	Qualitative bone growth analysis . . . . .	3
Figure 2.	FTY720 bioactivity and release from PLAGA coated graft . . . . .	3
Figure 3.	Polymer coated subperiosteal implant . . . . .	7
Figure 4.	Bone growth and remodeling in cranial defect with allograft. . . . .	8
Figure 5.	Allograft-host bridging and void space bone growth analysis. . . . .	9
Figure 6.	Histology of cranial defect with allograft . . . . .	10
Figure 7.	Monocytes in peripheral blood of allograft study . . . . .	12
Figure 8.	SMA+ blood vessels in allograft and cranial defect area. . . . .	13
Figure 9.	Allograft study vascular network MICROFIL analysis. . . . .	13
Figure 10.	Directly adsorbed FTY720 release from human trabecular graft. . . . .	14
Figure 11.	Bone growth and remodeling in cranial defect with xenograft. . . . .	14
Figure 12.	Change in bone volume in xenograft and cranial defect area. . . . .	15
Figure 13.	Xenograft and defect area vascular network visualization. . . . .	16
Figure 14.	Xenograft and defect area blood vessel volume analysis. . . . .	18

## **List of Symbols/Abbreviations**

BMP: Bone morphogenetic protein

BSA: Bovine serum albumin

CD11b: Cell surface receptor found on polymorphonuclear leukocytes, NK cells and mononuclear phagocytes

CD34: Human single pass transmembrane protein on early hematopoietic and vascular-associated cells

CD45: Leukocyte common antigen receptor

FTY720: Immunomodulating drug that is S1P<sub>1</sub>, S1P<sub>3</sub>, S1P<sub>4</sub> and S1P<sub>5</sub> agonist

MicroCT: Micro-computed tomography

PBS: Phosphate buffered solution

PLAGA: Poly(lactic-co-glycolic acid)

SBF: Simulated body fluid

S1P: Sphingosine 1-phosphate

S1P<sub>1-5</sub>: G-protein coupled sphingosine 1-phosphate receptors 1-5

SD: Genetically and functionally wild type Sprague Dawley rat.

## Introduction

Bone graft procedures number over 500,000 annually in the United States, with graft tissue used for 33% of the bone graft operations in 1996 (Boyce 1999). To address the growing clinical demand for effective bone reconstruction materials, bone graft substitute (graft) from cadavers and donors have been utilized extensively to repair skeletal defects. Though autologous bone grafts are superior to that of various other bone substitutes for bone reconstruction (Giannoudis 2005; Mokbel 2008), the graft mass is inadequate for massive bone defects. Bone harvesting leads to significant donor site morbidity in nearly one third of patients (Younger 1989), increased surgery time, and another potential infection site. Allografts avoid these problems, and their biocompatibility and osteoconductivity are superior to synthetic bone substitute materials (Delloye 2007). The American Association of Tissue Banks and Food and Drug Administration guidelines and bank accreditations give a vital safety assurance against risks of transmitting bacterial infection, hepatitis, HIV, or other diseases (American Academy of Orthopaedic Surgeons. 2011). However, poor remodeling and lack of vascularization of the processed bone graft can lead to failure from recurring infection, fracture, or nonunions (Delloye 2007; Thompson 1993; Enneking 2001; Mankin 2005). Complications associated with cadaver graft occur 30-60% of the time for massive transplants (Delloye 1988; Friedlaender 2006). Grafts can lose 50% strength after ten years *in vivo* (Wheeler 2005), although most failures occur within the first four years (Friedlaender 2006).

Cell augmentation, graft processing and use of bone morphogenetic proteins (BMPs) have been explored as possible means to increase graft incorporation in the

defect site. Johnson showed that hBMP in an allogeneic, autolysed antigen-free bone graft provided a good structural and delivery system for inducing bone formation by causing internal remodeling following femoral reconstruction after failed fracture healing. However, they supplemented all defects greater than 2 cm with an autogenic bone graft (Johnson 2000); in settings such as difficult nonunion of a long bone, the graft size need may be more than is possible due to BMP's available quantities (Friedlaender 2006). BMP-2's relatively short elimination half-life of 5.6 days while locally administered in a collagen carrier (Sellers 2000) has been a major drawback when used to coat off-the-shelf acellular constructs like grafts because the limited bone remodeling in a critical size defect occurs over months. One recent approach to counteract this limitation has been to use grafts coated with freeze-dried self-complimentary AAV-2.5 BMP-2 adeno-associated virus (Yazici 2011). Local, sustained physiologic levels of BMP-2 resulted in higher strength and bone volume compared to both graft and autograft treatments. However, the simplicity of small molecules compared to biologic therapies make pursuing alternative treatments worthwhile.

It is well established that graft vascularization and new bone formation are critical for graft survival and incorporation. Significant interest has emerged in the development of technologies to enhance the integration and efficacy of processed cadaver grafts used for bone reconstruction by promoting rapid vascularization upon implantation, as well as by encouraging the recruitment of endogenous host stem and progenitor cells. Several factors such as the presence or absence of living, histocompatible, committed bone-forming cells (Stevenson 1996), embryological mode of development and the quantity of cancellous bone (Pinholt 1994) have been suggested to have an influence on the

vascularization, and hence engraftment of the bone grafts. To this effect, this work continues to investigate the effects of local, sustained delivery of sphingosine 1-phosphate (S1P) receptor targeted drugs to induce neovascularization and improve healing outcomes in tissue engineering. S1P is an autocrine and paracrine signaling small molecule that is known to affect proliferation, survival and migration of endothelial cells, mural cells (i.e. vascular smooth muscle cells and pericytes), osteoblasts, and osteoblastic precursors through a family of high-affinity G protein-coupled receptors (S1P<sub>1-5</sub>) (Zhang 1991; Cuvillier 1996; Lee 2001; Ryu 2006; Pebay 2007). S1P has also been shown to enhance angiogenesis and vascularization in various pre-clinical models in addition to regulating B and T cell trafficking and the egress of immune cells from lymph nodes (Schwab 2005; Pappu 2007).

In previous work, it was shown that sustained release of S1P and FTY720, an S1P<sub>1</sub> and S1P<sub>3</sub> agonist, from biodegradable poly(DL-lactic-*co*-glycolic acid) (PLAGA) promotes microvascular network growth and arteriolar expansion (Sefcik 2011). It was also shown that the local delivery of FTY720 from PLAGA film promotes local microvasculature formation and cranial defect healing in a rat model (Petrie Aronin 2010a; Huang 2012). Superior osseous integration across the host-graft interface, enhancement of mechanical properties, increased smooth muscle cell investment, and reduction in leukocyte recruitment was also evident in FTY720-treated groups in a rat tibial defect model (Petrie Aronin 2010b). FTY720, a small molecule drug that modulates S1P receptors, is more stable and has a longer half-life than many growth factors that are candidates for clinical applications. FTY720 has been FDA approved as an oral drug for treatment of multiple sclerosis (Sharma 2011). FTY720 has been efficiently loaded in

PLAGA microsphere scaffolds and degradable implant coatings to ensure that the drug is released for several weeks following implantation. Critical size cranial defects have been used to examine the efficacy of drugs and other potential therapies for maxillofacial nonunions (Schmitz 1986). However, studies with subperiosteal implants help provide initial insights into revascularization and bone regeneration qualities of the implant (Chen 1994).

In this study, FTY720 coating efficacy on cranial subperiosteal implants was explored, and then a semicircular calvarial drug loaded, polymer coated allograft was used to evaluate total bone volume growth, bone remodeling at the interface, and directed bony ingrowth into the defect area. FTY720's effect on increased vascularization, arteriogenesis, and progenitor cell recruitment in the defect area was also explored. The therapy was then expanded to remove the polymer vehicle by directly adsorbing FTY720 to the bone graft; this delivery system was similarly tested for efficacy.

## Materials and Methods

To explore the potential of drug releasing grafts to integrate with the host and promote bone growth, FTY720 loaded in PLAGA coated, PLAGA coated only, or uncoated allografts were implanted in rat calvarial subperiosteum. Subsequent to the subperiosteal implant study, a semicircular graft for the rat critical size cranial defect model was developed. The bone graft was placed on one side, allowing measurement of both host-graft bridging and integration and bone induction into the defect void space. Calvarial bone allografts were loaded with FTY720 through a PLAGA coating. Human bone xenografts were loaded with FTY720 through direct adsorption. FTY720 encapsulation and release was quantified *in vitro* for both methods. FTY720 effects on total bone volume, bone growth qualities, blood vessel network growth, and circulating blood cells were explored for both cranial defect studies.

### *Bone Graft Harvest*

Parietal bone was harvested from wild type Sprague Dawley (SD) female rat skulls (4-5 months old), trimmed to a rectangular shape (5.7x5.2x0.75 mm<sup>3</sup>) and used in the subperiosteal implantation. The cranial defect allograft study used parietal bones from 8-week-old SD female rats, trimmed to two semi-circles ( $\approx$ 5 mm diameter edge along the sagittal suture). Allografts were stripped of soft tissue, cleaned with detergent, hydrogen peroxide, and ethanol sonication washes, and then allowed to fully dry (DePaula 2005). The xenograft study used human femur trabecular bone provided and cleaned by LifeNet Health® with their patented Allowash XG® process. The xenografts were cut in semi-circles 8 mm in diameter and 1 mm in thickness. All bones were analyzed with micro-

computed tomography (microCT) vivaCT40 scanner (SCANCO Medical AG, Brüttisellen, Switzerland) for volume, weighed, and equally divided into treatment groups. Samples were stored at -20°C until use.

### *Bone Graft Drug Loading*

Polymer coatings used 50:50 poly(lactic-*co*-glycolic acid) (PLAGA; 69.85 kDa; Lakeshore Biomaterials, Birmingham AL) dissolved in dichloromethane at 1:12 (w:w) in a 15 mL scintillation vial. For drug loading, FTY720 (343.9 Da; Cayman Chemical, Ann Arbor MI) was agitated until dissolved in the polymer solution at either 1:200 or 1:40 of drug to polymer (w:w). To coat allograft samples, bones were gently vortexed in polymer coating solution for 10 minutes. For directly adsorbed FTY720 bone xenografts, 1.5 mg FTY720 was dissolved in 0.6 mL methanol in a 4 mL scintillation vial; bone xenografts were gently vortexed in the drug solution for 4 hours. All bones were kept at 4°C for 24 hours to dry, and then lyophilized for 24 hours to extract remaining solvent (Labconco Corp., Kansas City MO).

### *FTY720 Loading Efficiency and Release*

FTY720 quantities were measured by sphingolipid extraction from solution and HPLC-MS. For polymer coated extraction efficiency, FTY720 was loaded 1:200 drug: polymer (w:w) and 1:12 polymer: solvent (w:v) onto calvarial allografts; coated grafts were dissolved in the first step of sphingolipid extraction and the bone was removed before further extraction was done. For the directly adsorbed FTY720 xenograft loading efficiency, pre-coating and post-coating solution samples were collected and analyzed.

For sphingolipid extraction, solutions were sonicated with chloroform (0.5 mL) and methanol (1.5 mL). To measure extraction efficiency, a *D-erythro*-Sphingosine (C-17 base) internal standard was added (30  $\mu$ L, 1  $\mu$ M, Mw=285.47 Da; Avanti Polar Lipids, Inc., Alabaster AL). This mixture was sonicated for 10 minutes, and immediately incubated at 48°C for 16 hours. After cooling to room temperature, KOH (0.2 mL, 1 M) was added, and the solution was centrifuged at 10,000xg for 10 minutes at 4°C. The supernatant was collected, dried to a solid with nitrogen air-flow, and stored at -20°C. Immediately prior to HPLC-MS analysis, the extraction residue was dissolved in methanol (0.3 mL) and centrifuged at 12,000xg for 12 minutes at 4°C to acquire the supernatant for analysis. Samples were analyzed with a Shimadzu UFLC High Performance Liquid Chromatograph (Columbia, MD) equipped with a Supelco Discovery C18, 5 $\mu$ m (125 $\times$ 2 mm) connected to an ABI 4000 QTrap triple quadrupole mass spectrometer (Applied Biosystems, Inc., USA).

For *in vitro* release, grafts were placed in 4 mL scintillation vials containing simulated body fluid (pH 7.2; 7.996 g NaCl, 0.35 g NaHCO<sub>3</sub>, 0.3 g KCl, 0.136 g KH<sub>2</sub>PO<sub>4</sub>, 0.095 g MgCl<sub>2</sub>, 0.278 g CaCl<sub>2</sub>, 0.06 g MgSO<sub>4</sub> in 1 L deionized water) with 4% (w:v) fatty acid free bovine serum albumin (SBF-BSA), and incubated at 37°C with constant agitation. Coated allografts were placed in 1 mL SBF-BSA; each day for 5 days, the bone was moved to a new vial with fresh solution. Adsorbed xenografts were placed in 0.5 mL SBF-BSA; release was carried out for a total of 4 weeks with solutions changed and collected at day 0.17, 1, 2, 7, 15, 22, and 29. FTY720 was extracted from incubation solutions and quantified as described above.

### *Polymer Coating Released FTY720 bioactivity*

To ensure FTY720 remained functional after being loaded and released from the allograft, the *in vitro* release was repeated to obtain the FTY720 released from coated grafts each day for 5 days; these samples underwent sphingolipid extraction in order to be used in a sphingosine kinase 2 (SPHK2) assay. Briefly, this assay uses SPHK2 and radioactively labeled ATP to phosphorylate FTY720 into FTY720-<sup>32</sup>P; thus, intact FTY720 which can be phosphorylated as in the body is counted by radioactive activity. To prepare recombinant SPHK2, mouse SPHK2 cDNA was cloned in pcDNA3.1 vector and expressed in HEK293T cells by transfection. After 2 days, cells were harvested by scraping into a kinase buffer consisting of 20mM Tris-Cl (pH 7.4), 1 mM 2-mercaptoethanol, 1 mM EDTA, 5 mM sodium orthovanadate, 40 mM  $\beta$ -glycerophosphate, 15 mM NaF, 1 mM phenylmethylsulfonyl fluoride, 10 mM MgCl<sub>2</sub>, 0.5 mM 4-deoxypyridoxine, 10% glycerol, and 0.01 g/L each leupeptin, aprotinin, and soybean trypsin inhibitor; the cells were then disrupted with a Dounce homogenizer. The homogenate was clarified by centrifugation at 15,000 rpm, aliquoted, and stored at -20°C until use.

SPHK 1 and 2 activity was measured in the kinase buffer. To determine the fractional activity of SPHK1 versus SPHK2, the kinase buffer was supplemented with either 0.5% Triton X-100 or 1 M KCl, respectively. To label FTY720, the kinase buffer was supplemented with FTY720, [ $\gamma$ -<sup>32</sup>P]ATP (10  $\mu$ M, specific activity=8.3 Ci/mmol), 200  $\mu$ M KCl and recombinant SPHK2. After 30 min at 37 °C, the reaction mixture was extracted with 2 volumes of chloroform/methanol/HCl (100:200:1), and the components in the organic phase were separated by thin layer chromatography using a 1-

butanol/acetic acid/water (3:1:1) solvent system. Radiolabeled enzyme products were detected by autoradiography and identified by migration relative to authentic standards. The silica gel containing radiolabeled lipid was scraped into a scintillation vial and quantified with a Beckman Coulter LS 6500 liquid scintillation counter.

### *Subperiosteal Implant and Cranial Defect Surgeries*

All animal surgeries were performed according to an approved protocol from the University of Virginia Animal Care and Use Committee. All animals were obtained from Charles River Laboratories International, Inc. (Wilmington MA). In the subperiosteal implant study depicted in Figure 1a, female SD rats ( $\approx 270$  g) were randomly assigned to three different experimental groups (n=4): uncoated graft, PLAGA coated, and 1:200 FTY720 loaded. Anesthesia was induced with isoflurane gas and continued with Ketamine/Xylazine (80/8 mg/kg IP). Following anesthetization, the dorsal skin was sterilized with Betadine and 70% ethanol. The longitudinal incision was performed over the dorsum of the skull over the sagittal suture and was made through skin and periosteum. Periosteum was elevated over the parietal and frontal bones to a diameter of 1 cm. The rectangular graft was placed underneath the periosteum, in direct contact with the parietal bone, centered on the sagittal suture, and between the coronal and lamboid sutures. The periosteum was closed with a 5-0 running nylon suture. The skin was closed with a running subcuticular vicryl suture, and VetClose™ (Butler Animal Health Supply, Dublin OH) was applied on the incision. Ketoprofen (3 mg/kg SC) was given after closure and then as needed (once a day) to minimize post surgery pain. Rats were given free access to food and water and monitored for complications or abnormalities. At 4

weeks post-surgery, rats were anesthetized with 2.5% isoflurane gas and injected in the heart with 1 mL Nembutal.

In the allograft cranial defect study shown in Figure 1b, female SD rats ( $\approx 220$  g) were randomly assigned to four groups (n=8) and euthanized 8 weeks post surgery: uncoated graft, PLAGA coated, 1:200 FTY720 loaded, and a higher FTY720 loading of 1:40. In the xenograft cranial defect study, female SD rats ( $\approx 235$  g) were randomly assigned to three groups (n=3) and euthanized 12 weeks post surgery: empty defect, xenograft, and FTY720 loaded xenograft. Animal anesthesia, preparation, post-surgical care, and euthanasia were performed as explained above. A longitudinal incision was made through the skin and periosteum, directly over the sagittal suture. Periosteum was elevated over the parietal and frontal bones to a diameter of 1 cm. A 3 mm round burr was used to create an 8 mm defect in the bone with constant saline irrigation using a Hall® Surgical E900® System and Coolflex® High Speed Drill (CONMED Linvatec, Largo FL). Thin bone chips still adherent to the dura were carefully elevated with a round knife and removed. The defect was then smoothed with a 1 mm diamond burr. The graft was placed into the defect, and the periosteum was closed over the implant with a 5-0 running nylon suture. The skin was closed with a running subcuticular vicryl suture, and VetClose™ was applied over the sutured area.

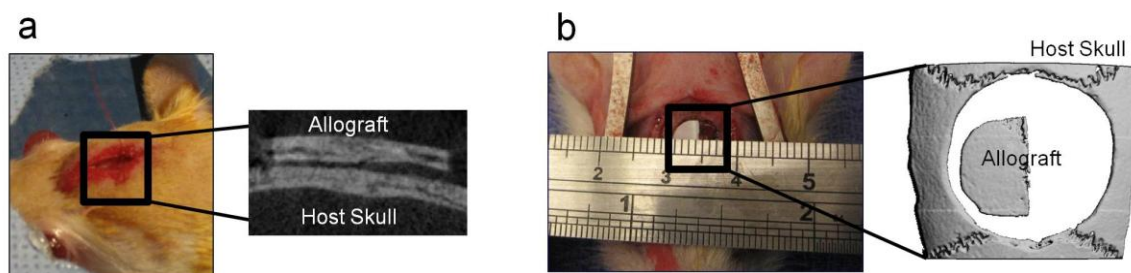


**Figure 1.** Rat subperiosteal implant and critical size cranial defect models. a) Polymer coated allografts were placed under the periosteum in a pocket created by blunt dissection and sutured into position flush to the host calvaria. b) Semi-circular bone grafts were placed in a critical size cranial defect so one edge was close to the host bone, and a void space was left to explore the induced bone growth response to the graft.

#### *MicroCT Imaging of Bone and MICROFIL®*

Grafts and animals were imaged using the quantitative microCT. Grafts were scanned with the following parameters: 21  $\mu\text{m}$  voxel size, 55 kVp, 145  $\mu\text{A}$ , medium resolution, 21.5 mm diameter field of view, and 200 ms integration time. Animals were scanned with the following parameters: 38  $\mu\text{m}$  voxel size, 55 kVp, 145  $\mu\text{A}$ , medium resolution, 38.9 mm diameter field of view, and 200 ms integration time (73 mGy radiation per scan). Rats were scanned biweekly under anesthesia until euthanasia time point. 2D images were segmented by drawing the region of interest to comprise only parietal bone by including all bone inside the ridges separating parietal from temporal bone. Slice number was set for each animal throughout the study to include the whole defect and an equal length both anterior and posterior of the defect ( $\approx 272$  slices). Bone was thresholded at 481.3-2000 mg hydroxyapatite (HA)/ $\text{cm}^3$ , and bone volume was measured with the microCT software.

Following end time point *in vivo* scans for cranial defect rats, all cranial blood vessels were perfused with MICROFIL® MV-122 (Flow Tech Inc., Carver MA) to image and quantify with microCT (n=3 at each time point). Rats were euthanized, the heart was exposed, and the common carotid arteries were cannulated. The right atrium was incised to allow drainage. Ligating the arteries below the cannulation points allowed direct perfusion of the vasculature in the neck and head region with 2% heparin-saline from both sides simultaneously with syringe pumps; each side was perfused with 5 mL in 12.5 minutes. Then 2.5 mL MICROFIL® mixed 1:1 with diluent was perfused from each side in 12.5 minutes. The solution was allowed to set for 16 hours at 4°C. The calvarial sample including the defect and the surrounding parietal bone was harvested, fixated, and decalcified as described in the following section. Following decalcification, allograft cranial defect samples were scanned in air with the following parameters: 21  $\mu\text{m}$  voxel size, 45 kVp, 177  $\mu\text{A}$ , medium resolution, 21.5 mm diameter field of view, and 200 ms integration time. Blood vessels in decalcified tissue were thresholded from 164-1500 mg HA/cm<sup>3</sup>, and the total blood vessel volume was quantified within a 8x9 mm<sup>2</sup> area centered at the defect. The sagittal sinus was excluded from the volume of interest due to its relatively large volume and variation between animals. The xenograft cranial defect samples were similarly scanned and analyzed, except the samples was cut to a 10x10 mm<sup>2</sup> area and scanned at high resolution.

3D volume renderings were either done with SCANCO software after segmentation, or OsiriX 3.9 (Pixmeo, Geneva, Switzerland) from DICOM files of the region of interest. OsiriX images were thresholded and colored appropriately with the 16 bit color look up table (CLUT).

*Polymer Coated Allograft Induced Bone Growth Qualitative Analysis*

Bone growth characterization in the cranial defect was organized into 2 types: 1) Graft incorporation and bridging along the interface and 2) Host bone healing response in the defect void space. This distinction was made possible by the use of semi-circular grafts in the defect region. Five animals were randomly chosen from each group, and their week 2 and 8 MicroCT 3D volumes were scored by at least four blinded evaluators compared to the week zero images. The left side of Table 1 below describes the evaluation of remodeling occurring at the interface on a grading scheme of 1-4, ranging from minimal growth to complete bridging across the entire width of the graft. Table 1's right side describes bone growth in the defect void region categorized according to amount, aspect ratio (width: height), and location. This growth was determined to be directed or undirected towards the graft through the growth aspect ratio. The results of this analysis were used to choose representative microCT 3D images.

**Table 1.** Qualitative bone growth diagrammatic representations and scoring descriptions.

Score	Host-Graft Interface Growth	Category	Bone Growth Description
1	Minimal growth at the interface or only graft resorption	A	Longer, undirected growth from or near defect edge (right of line)
2	Obvious but un-bridged growth at the interface	B	Longer, undirected growth closer to the graft (left of line)
3	Less bridging growth at interface (left of dashed line)	C	Wider growth towards graft from or near defect edge (right of line)
4	More bridging growth at interface (both sides of dashed line)	D	Wide growth from edge through the void space (crosses line)

### *Histology and Immunohistochemistry*

Following *ex vivo* microCT scanning, calvarial samples were fixed in 10% buffered formalin for 7 days and decalcified using an HCl and EDTA decalcifying solution (Richard-Allan Scientific, Kalamazoo MI) for 3 days at 4°C with agitation. The parietal bone was cut in half, perpendicular to the sagittal suture and centered at the defect or implant. The rostral half was stored in 70% ethanol until paraffin embedding for hematoxylin and eosin (H&E) and Masson's trichrome staining. The caudal half was flash frozen in Tissue-Tek O.C.T. and cryo-sectioned for  $\alpha$ -smooth muscle actin (SMA) staining to visualize mature vessel lumens. Frozen sections were washed (PBS, 0.1% saponin), blocked for 30 minutes (PBS, 0.1% saponin, 2% bovine serum albumin (BSA)), and immunolabeled for 16 hours at 4°C with monoclonal Anti-Actin,  $\alpha$ -Smooth Muscle - Cy3<sup>™</sup> murine antibody (Sigma Aldrich) diluted 1:500 in (PBS, 0.1% saponin, 0.1% BSA). Labeled sections were then washed and mounted with PBS and glycerol solution (1:1). To quantify changes in vascular remodeling, particularly the recruitment of mural cells, in response to FTY720, obvious lumen formed by SMA+ cells was quantified in each tissue section.

### *Blood Cell Collection and Analysis*

Circulating blood monocyte levels in allograft implanted cranial defect animals were quantified immediately, 1 week, and 2 weeks after surgery. The rat's tail vein was incised to achieve a slow, steady bleed. After the first blood was wiped with gauze, 200  $\mu$ L blood was drawn and mixed with 10  $\mu$ L EDTA (0.5 M). This solution was sampled, and quantified with HEMAVET® 950FS (Drew Scientific Group, Waterbury CT).

### *Statistical significance*

Results are presented as mean  $\pm$  standard error of the mean. All statistical analysis was performed using a one-way General Linear ANOVA, followed by Tukey's test for pairwise comparisons with Minitab 16 (Minitab Inc., State College PA). Significance was asserted at  $p < 0.05$  unless otherwise stated.

## Results

### *FTY720 loading, release, and bioactivity from polymer coating*

To quantify and characterize the nature of the polymer coated allograft drug delivery system, *in vitro* release products from PLAGA coated, FTY720 loaded (1:200 drug: PLAGA) grafts were collected and analyzed either with sphingosine kinase 2 assay for bioactivity or with a HPLC-MS for quantity. Figure 2a shows the bioactivity of the released FTY720 after being loaded in the polymer coating. SPHK2 normally phosphorylates the pro-drug FTY720 *in vivo* to FTY720-P, which then acts as a potent agonist for selective S1P receptors. In this assay, only FTY720 able to react with SPHK2 is phosphorylated with radioactive  $^{32}\text{P}$ -ATP and measured. Quantified cumulative FTY720 release over 5 days showed a relatively high amount after 1 day, and steady additional release each day after (Figure 2b). After 5 days, the PLAGA coating released over 50% (2.4  $\mu\text{g}$ ) of the encapsulated FTY720 (4.5  $\mu\text{g}$ ). The release profile closely follows the amount of FTY720 released and labeled in Figure 2a.

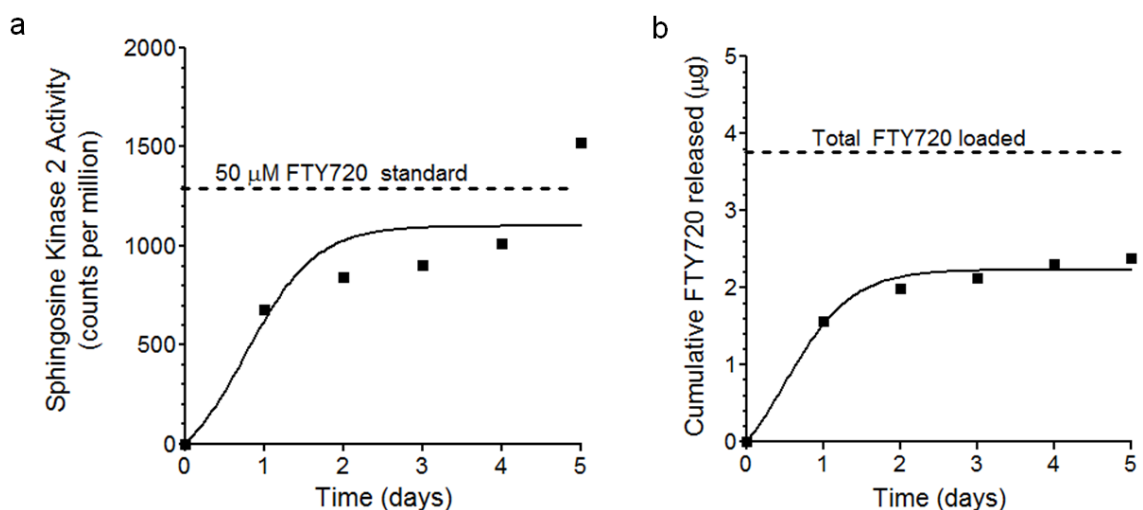


**Figure 2.** FTY720 bioactivity and release from PLAGA coated calvarial graft. a) After release, pro-drug FTY720 could be phosphorylated and radiolabeled at detectable levels with a sphingosine kinase 2 assay. b) FTY720 released from graft *in vitro* quantified with HPLC-MS (1:200 loading). FTY720 quantity released after one day has been shown to promote vascular remodeling *in vivo*.

### *Subperiosteal Implant Induction of Bone Growth*

Subperiosteal bone implants after 4 weeks are shown in Figure 3 as *ex vivo* MicroCT 3D renderings with arrows highlighting new bone formation in the interfacial space between the graft and host skull. FTY720 loaded grafts induced bridging bone growth all along the surface, while controls only saw the occasional raised bone mass from the skull. Masson's trichrome staining of the same samples highlights the bone bridging in the interfacial space of FTY720 grafts, while controls had slight growth only at the edges where the distance from graft to host bone was the shortest.

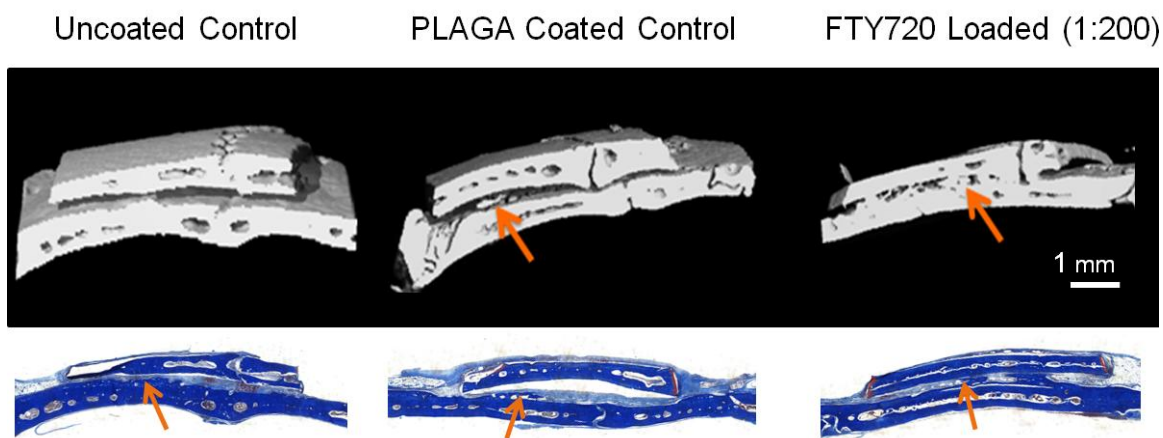


**Figure 3.** Qualitative assessment of subperiosteally implanted graft integration with host calvaria. 1:200 FTY720-loaded grafts had more interfacial bone growth (highlighted with arrows) compared to Uncoated or Coated control groups. Representative images at week 4: A) MicroCT 3D renderings and B) Masson's trichrome staining.

### *Bone Growth and Graft Integration in Allograft Implanted Critical Size Cranial Defect*

Representative images of calvaria at weeks 0, 2, and 8 post-surgery for the three experimental conditions, as well as a higher loading of FTY720 in the polymer coating (1:40 w:w) are shown in Figure 4a. Both the uncoated and PLAGA coated controls had some bone growth along the side edges of the defect and minor remodeling of the graft. Bone regression around the host sagittal suture was common. In contrast, FTY720 groups had almost complete host-graft bone bridging as well as directed bone growth in the void

space. Induced bone growth was often drawn towards the graft's sagittal suture dentated edge, which has a higher surface area of bone, and therefore more drug-loaded polymer coating than other graft edges.

Total bone volume growth in, and directly around the defect is shown in Figure 4b for each biweekly time point. At week 2, FTY720 groups had more bone growth compared to controls. The higher dosage of FTY720 (1:40) accelerated bone growth significantly compared to both uncoated and coated controls, while the lower dosage of FTY720 (1:200) was significantly higher than the coated control. By 4 weeks, the lower dosage of FTY720 growth was only slightly higher than controls, and not significantly so. However, 1:40 FTY720 continued to accelerate bone volume growth and was significantly higher than coated control. Between weeks 4 and 6, the lower dosage of FTY720 (1:200) continued growth, while the 1:40 FTY720 group growth slowed down. Despite the fact that both FTY720 treatment groups maintained the higher growth trend, the difference was not significant. Between week 6 and 8, all groups saw minimal bone growth changes.

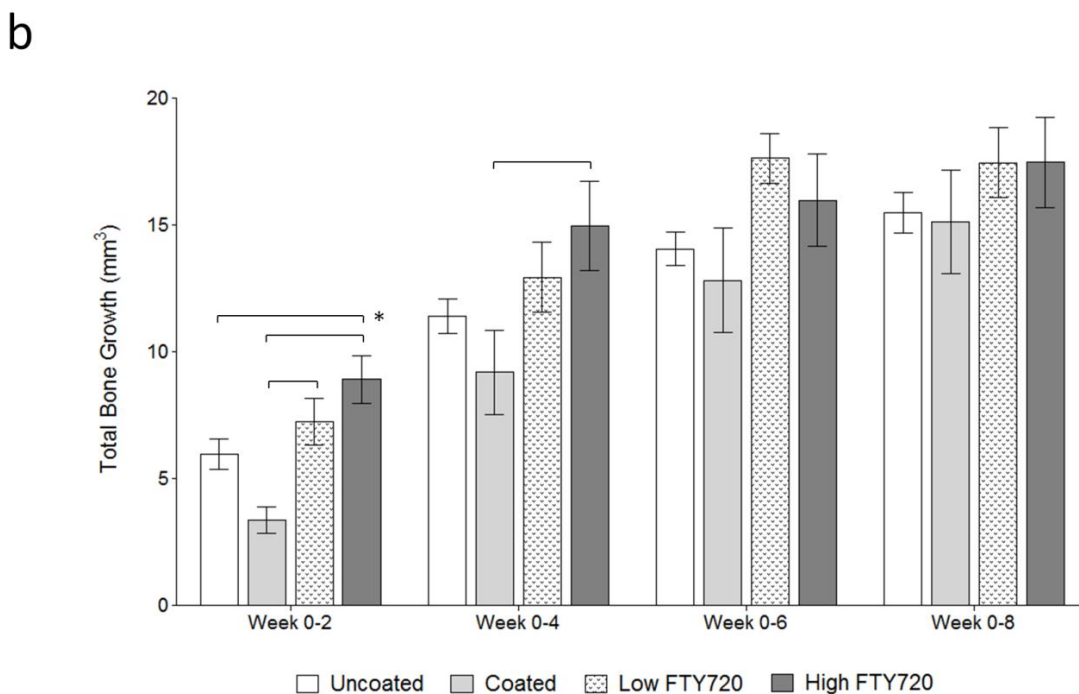
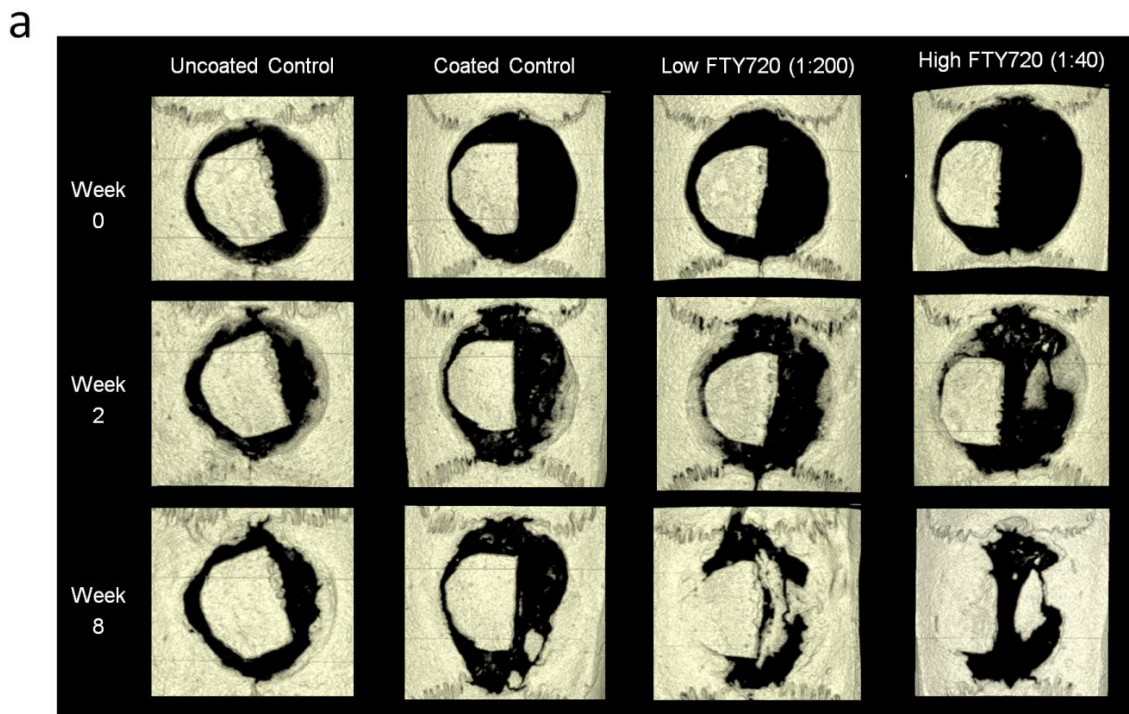


**Figure 4.** Bone growth and remodeling in cranial defect area over 8 weeks. a) Representative *in vivo* MicroCT shows FTY720 groups had improved host-graft bridging and directed bone growth in defect space. Controls had undirected bone growth at the defect edges. b) Quantification of total bone growth in and around defect at biweekly time points. FTY720 spurs a dose dependent bone healing response at weeks 2 and 4. By week 6, control group's growth increased while FTY720 groups' growth slowed. Bars indicate significance between groups ( $p < 0.05$  or  $*p < 0.10$ ).

To assess graft bridging at the host skull interface, as well as host bone growth response in the void space, qualitative bone changes were sorted into categories and evaluated as described in Table 1 of the Methods. Host-graft interface bone growth and bridging are characterized in Figure 5a for the four experimental groups. Healing from week 2 to 8 clearly increased interfacial growth. After 8 weeks, both FTY720 groups had host-graft interface bridging in 4/5 animals, compared to 2/5 and 3/5 in Uncoated and Coated controls, respectively. High FTY720 had the most animals with extensive integration (2/5). The bone growth pattern in the defect void space is characterized in Figure 5b at 2 and 8 weeks. At week 2, all groups except high FTY720 saw the majority (3/5) of animals with random growth at the far edge (category A). High FTY720 also had the highest number of animals with wider, directed growth on the defect void edge (category C). No group had any animals with extensive, directed growth. By week 8, there was a shift in the types of growth from random to directed growth towards the graft. FTY720 groups promoted extensive directed growth throughout the void from the far defect edge (category D). Controls had mostly random or less directed growth with 1/5 or fewer animals with extensive, directed growth.

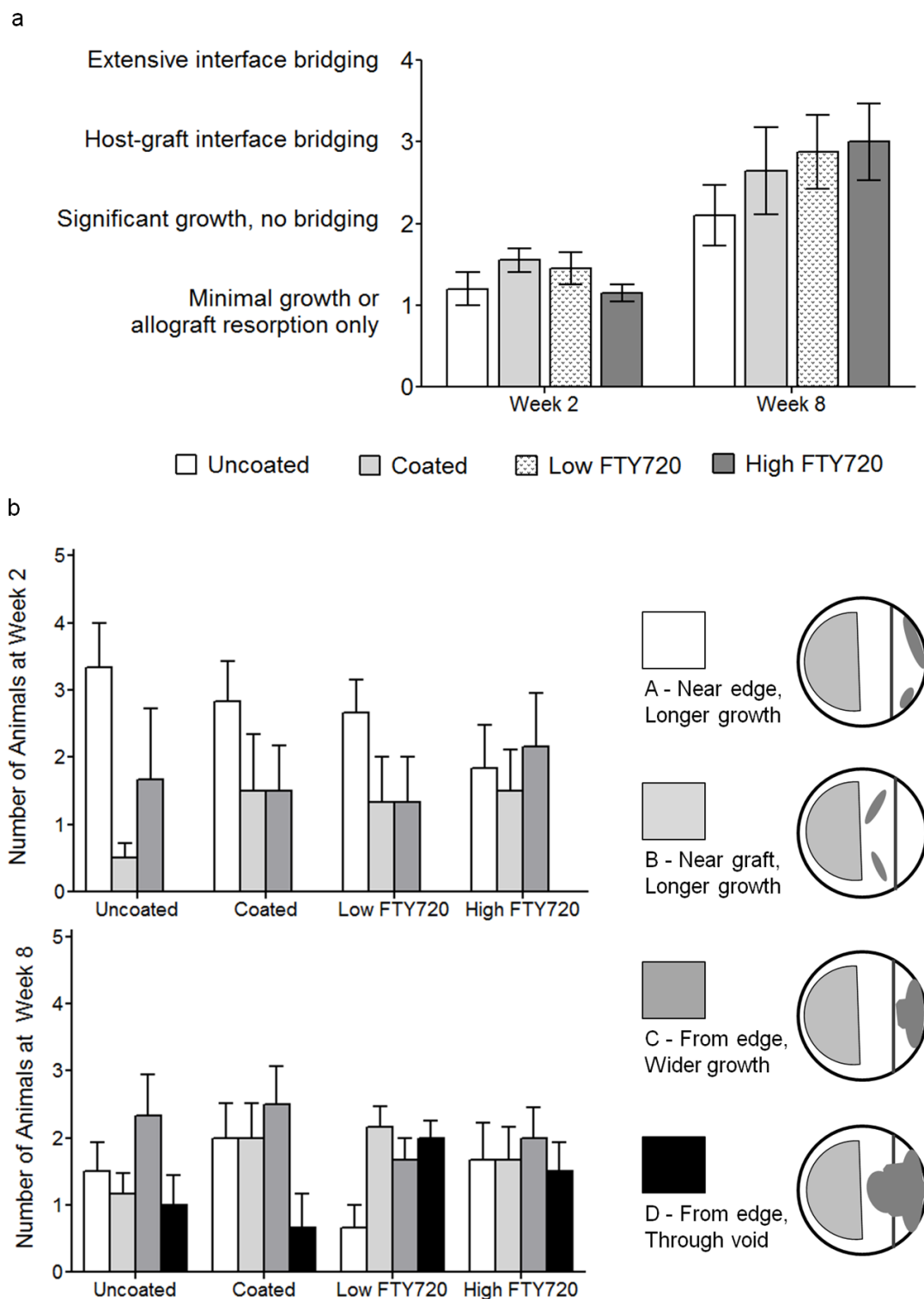


**Figure 5.** Qualitative analysis of bone growth and remodeling at the host-graft interface and in the defect void space. a) All groups saw increased bridging and growth from week 2 to 8. FTY720 loaded groups had the most extensive bridging. b) Defect void space growth was characterized through direction and location. All groups except for high FTY720 had mostly random growth along the far edge at week 2. By week 8, FTY720 groups had induced extensive directed growth towards the graft from the far edge of the defect.

Histological examination and evaluation of the cranial defect growth stained with H&E and Masson's trichrome after 8 weeks is shown in Figure 6. From whole tissue sections, the defect void space is still evident in control samples, and the tissue bridging the graft and host bone lacks mature cortical bone. In contrast, the FTY720 groups have mature bone formation at the opposite edge of the defect, in the original void space of the defect, and at the host-graft bridge (black box with white arrows showing bridging). The edges of the graft in control groups are clearly evident, and show less incorporation into native bone, compared to graft edges being well integrated in the FTY720 groups. From the Masson's trichrome stain, graft bone has been encapsulated with collagen matrix (light blue), denoting inclination for further calcification and strengthening. The presence of blood vessels (orange triangles) throughout the periosteum and soft tissue show the region is vascularized, which is a key feature for graft incorporation. Additionally, the presence of osteoclasts and osteoblasts (white triangles) indicate active remodeling in the region.

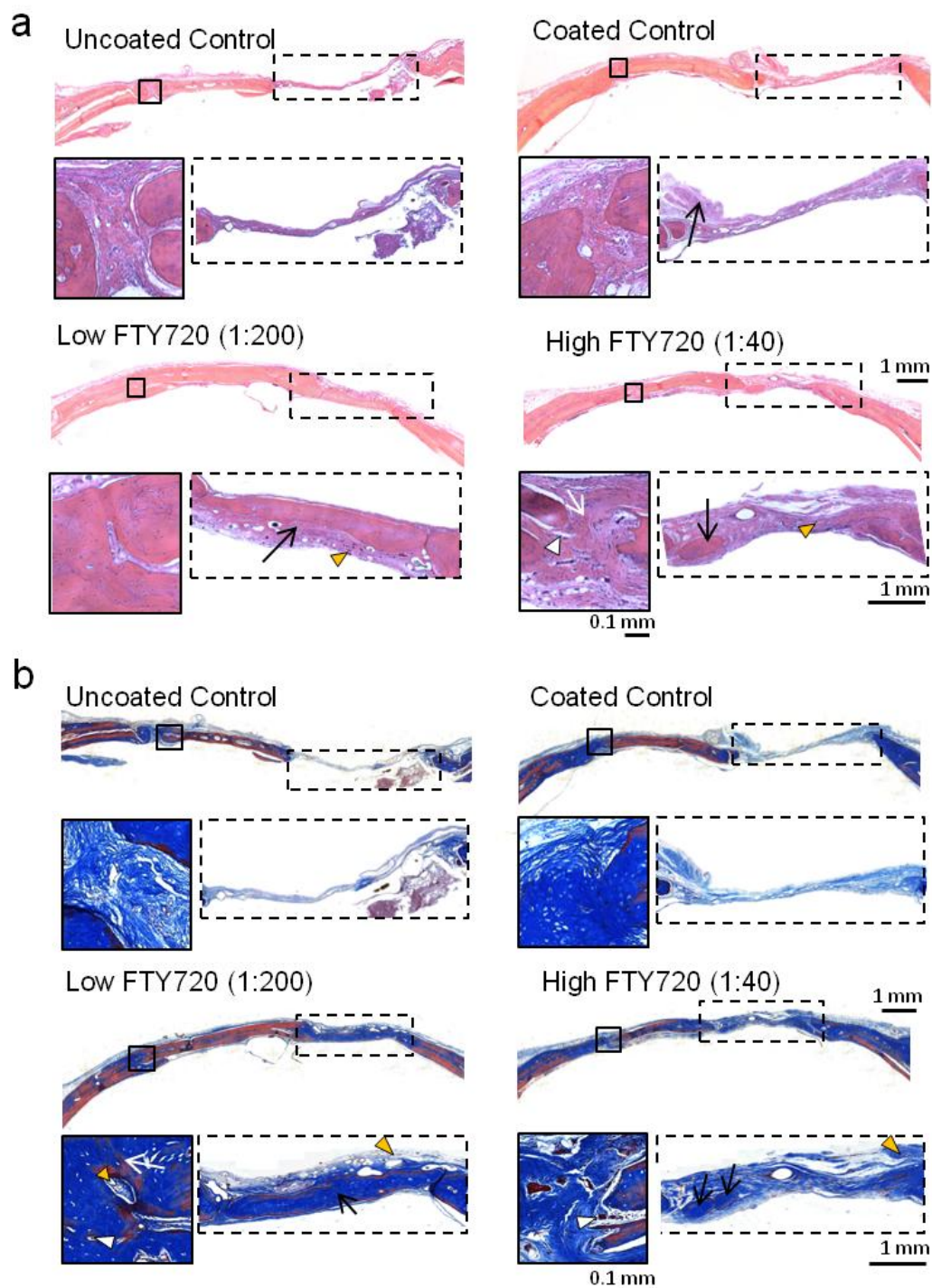


**Figure 6.** Histological analysis of cranial defect and graft area at week 8 with a) H&E and b) Masson's trichrome stain. In the FTY720 groups, the graft shows better incorporation with native bone tissue compared to controls. Host-graft interfacial bridging (black box) was successful in FTY720 groups (white arrow); similar bridging is absent in the control groups. Additionally, in the void space (dotted box), there is increased bone formation in the FTY720 groups compared to the uncoated control (black arrows). Vessel formation near the host-graft interface (orange triangles) and the presence of osteoids and osteoblasts stained dark brown (white triangles) also suggests active remodeling at the bone-graft interface.

To explore FTY720's systemic effect on circulating blood cells, and more specifically, osteoclast precursor recruitment, animal blood samples taken immediately after surgery, 1 week, and 2 weeks were analyzed for blood monocyte levels and represented in Figure 7 as percent change from week 0. After 1 week, high FTY720 loading resulted in statistically significant increased monocytes compared to controls, but they still remained within the normal range.

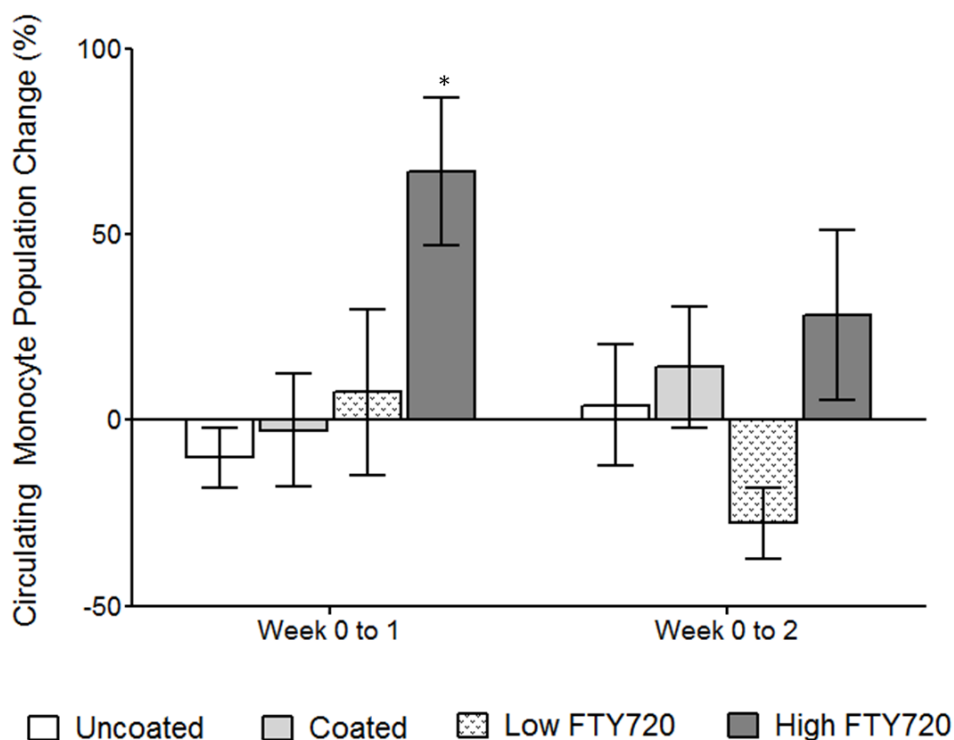


**Figure 7.** Monocytes in blood immediately after surgery and in the following weeks. High FTY720 loading leads to elevated circulating monocyte levels at both weeks one and two. \* indicates significance to all other groups ( $p < 0.05$ ).

#### *Blood Vessel Growth Evaluation in Allograft Implanted Defect*

Blood vessel growth and microvascular maturation are both vital for guiding and maintaining healthy bone growth. Smooth muscle cell investment and support of blood vessels was visualized with  $\alpha$ -smooth muscle actin (SMA) fluorescent labeling in cranial defect tissue sections and quantified. Figure 8a shows labeled images of the periosteum

region above the graft-void interface. Visible blood vessels with labeled smooth muscle cell support were mainly located in the periosteum and connective void tissue. Vessel lumen shape and diameter varied due to non-perpendicular orientation to the sectioning plane. Therefore, only the number of SMA<sup>+</sup> lumens was counted to represent the average total number of mature blood vessels bisecting the middle of the defect, as shown in Figure 8b. There was no significant difference between any groups at week 8.

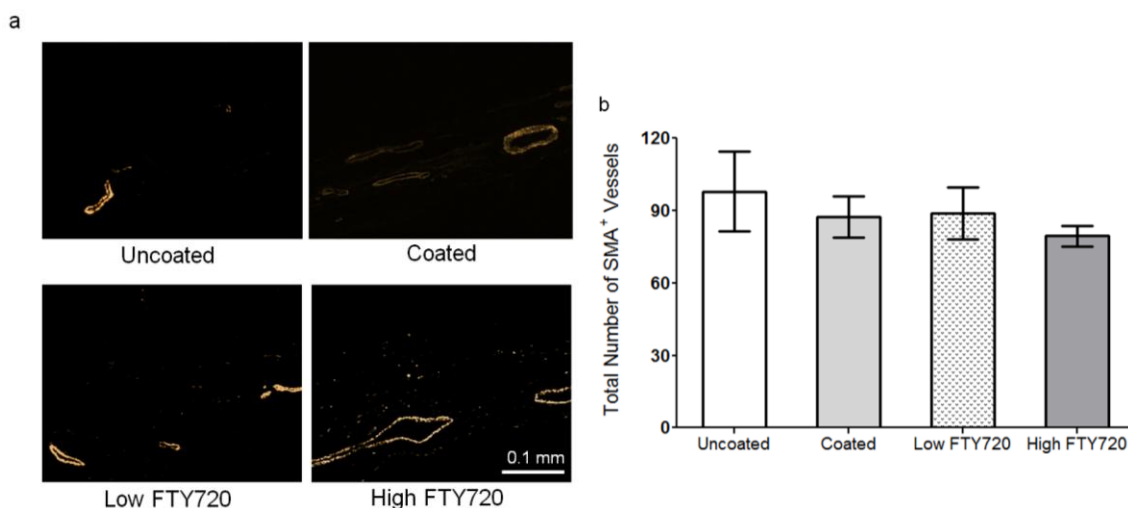


**Figure 8.** Fluorescent staining of SMA<sup>+</sup> blood vessels in the cranial defect area. a) Fluorescent images of SMA<sup>+</sup> blood vessels from the periosteum of the graft-defect interface are indicative of vessel formation and vascularization of the bone tissue. b) Quantification of the total number of SMA<sup>+</sup> blood vessels resulted in no significant difference between all groups at week 8 post surgery ( $p=0.73$ ).

To visualize and quantify the effect of FTY720 on the vascular response, the animal's head was perfused with radiopaque MICROFIL® and imaged with microCT. Representative 3D renderings of the blood vessel network (diameter > 20  $\mu\text{m}$ ) and the cranial defect area are shown in Figure 9a. From comparison of the blood vessel network and bone graft location, it appears that few blood vessels are able to penetrate the actual graft in all groups. In particular, the control groups had poor graft infiltration, as there are only visible blood vessels below the graft. However, the FTY720 groups appear to

have some vessel growth in the plane of the graft and periosteum. Figure 9b shows quantification of the total blood vessel volume in and around the graft area, excluding the sagittal sinus so its relatively large and inconsistent volume did not skew the data. Between the groups, there was no statistically significant difference in blood vessel volume in the whole area, on the graft side, or on the void side. By week 8, FTY720 effects on total blood vessel volume and total number of mature blood vessels have become indistinguishable from control groups through SMA<sup>+</sup> or MICROFIL® analysis. However, FTY720 appears to increase blood vessel investment specifically throughout the graft and the periosteum above the graft.

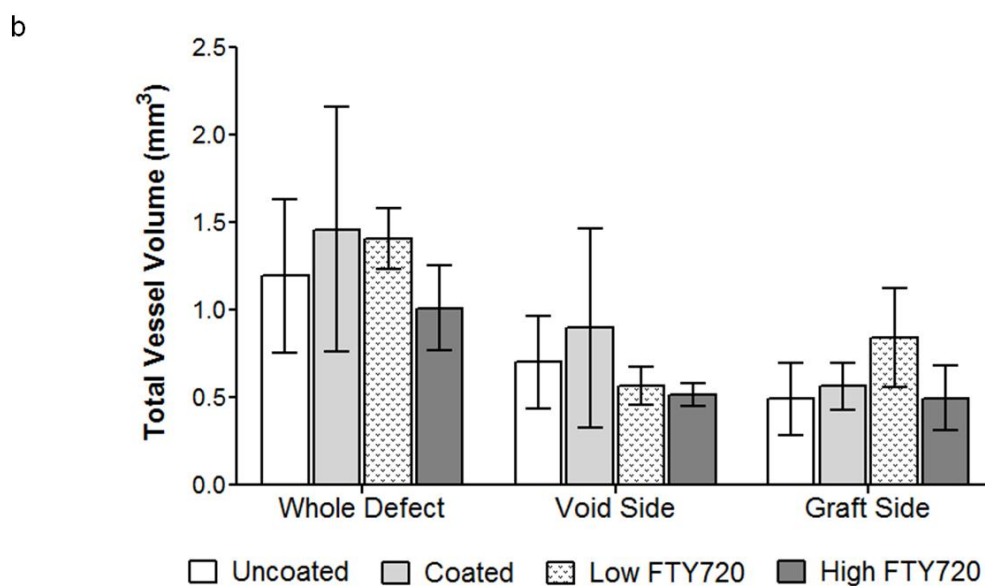
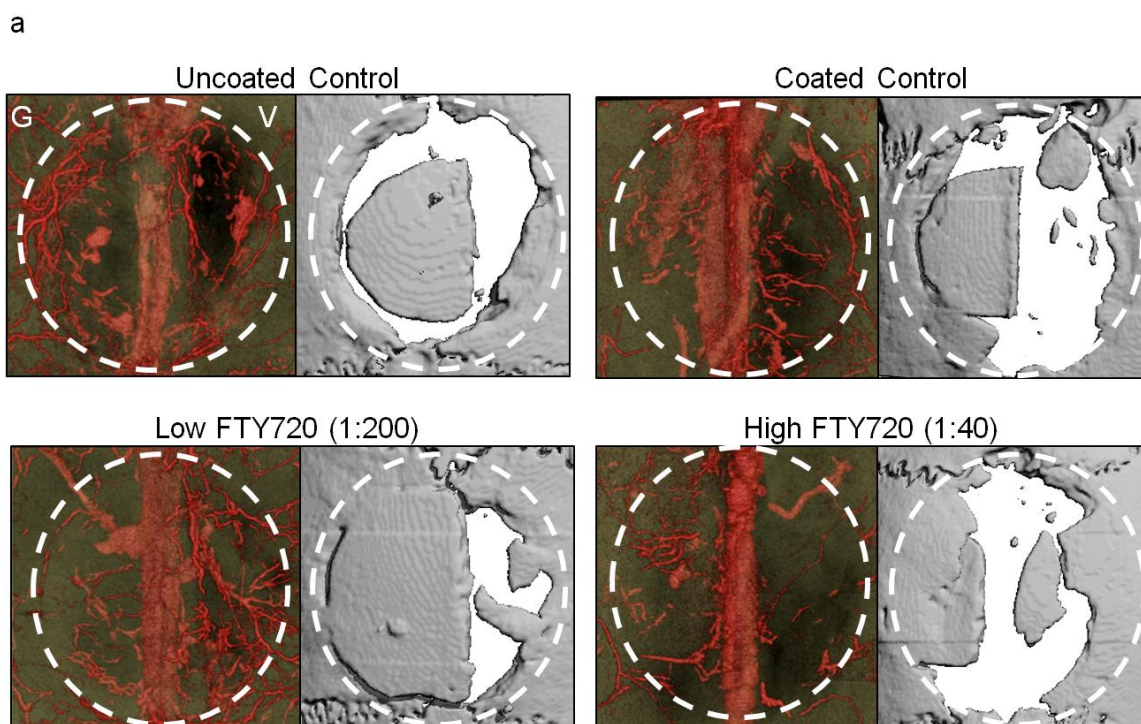


**Figure 9.** Total blood vessel growth in cranial defect area visualized with MicroCT imaging of a radiopaque agent. a) MICROFIL® perfused blood vessel network to visualize with MicroCT. Dotted circle approximates original defect, G is the graft side and V is the void side. b) Quantification of blood vessels (thresholding of 0-164 mgHA/cm<sup>3</sup>) showed by week 8, no significant difference was found among groups.

### *Directly adsorbed FTY720 loading and release*

To explore sustained drug delivery without a polymeric vehicle, FTY720 was directly adsorbed to a trabecular bone xenograft; *in vitro* loading solutions and release products were analyzed with HPLC-MS for quantity. Implanted xenografts had an average bone volume of 5.5 mm<sup>3</sup> and adsorption of 1,055 µg for a loading of 193 µg FTY720/mm<sup>3</sup> bone. The direct FTY720 adsorption release profile *in vitro* closely resembles the drug loaded polymer release as shown in Figure 10 below; drug release was sustained in a bone healing timeframe, with 0.9 µg FTY720 still being released during the fourth week. Initial release within the first four hours reached 15.8 µg, with release after the first day at 26.9 µg.

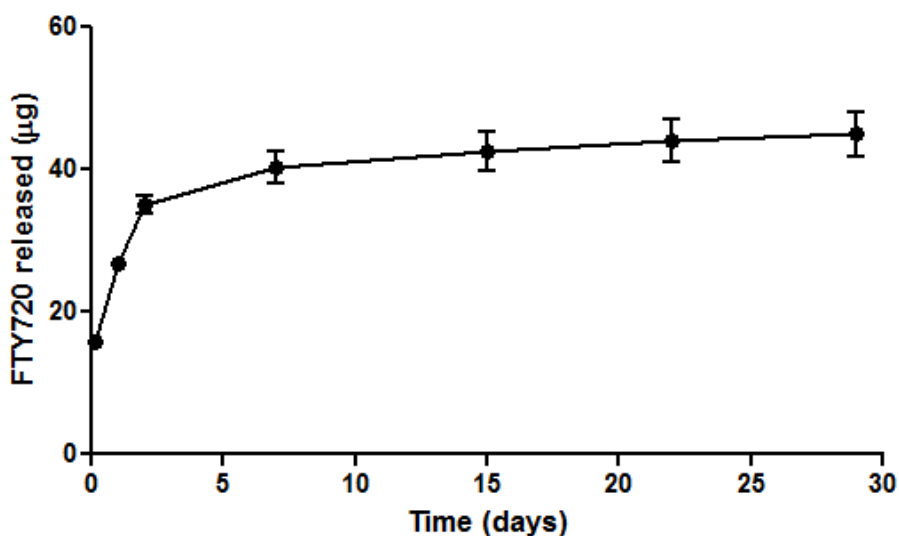


**Figure 10.** FTY720 *in vitro* release from bone xenograft quantified with HPLC-MS. Initial and continual release past four weeks can be reached at an order of magnitude higher than release from the PLAGA coating.

### *Bone Growth and Graft Integration in Xenograft Implanted Cranial Defect*

Representative images of calvaria at weeks 0, 4, 10, and 12 post-surgery for the empty, xenograft implanted, and FTY720 adsorbed xenograft implanted defects are shown below in Figure 11. FTY720 release spurred host bone ingrowth from all edges,

extensive graft remodeling, and the beginnings of graft bridging. By contrast, xenograft only saw sparse growth unevenly at the host edge, little graft remodeling, and random growth in the void space. Empty defect control had undirected bone ingrowth from the host edges and randomly in the defect space.

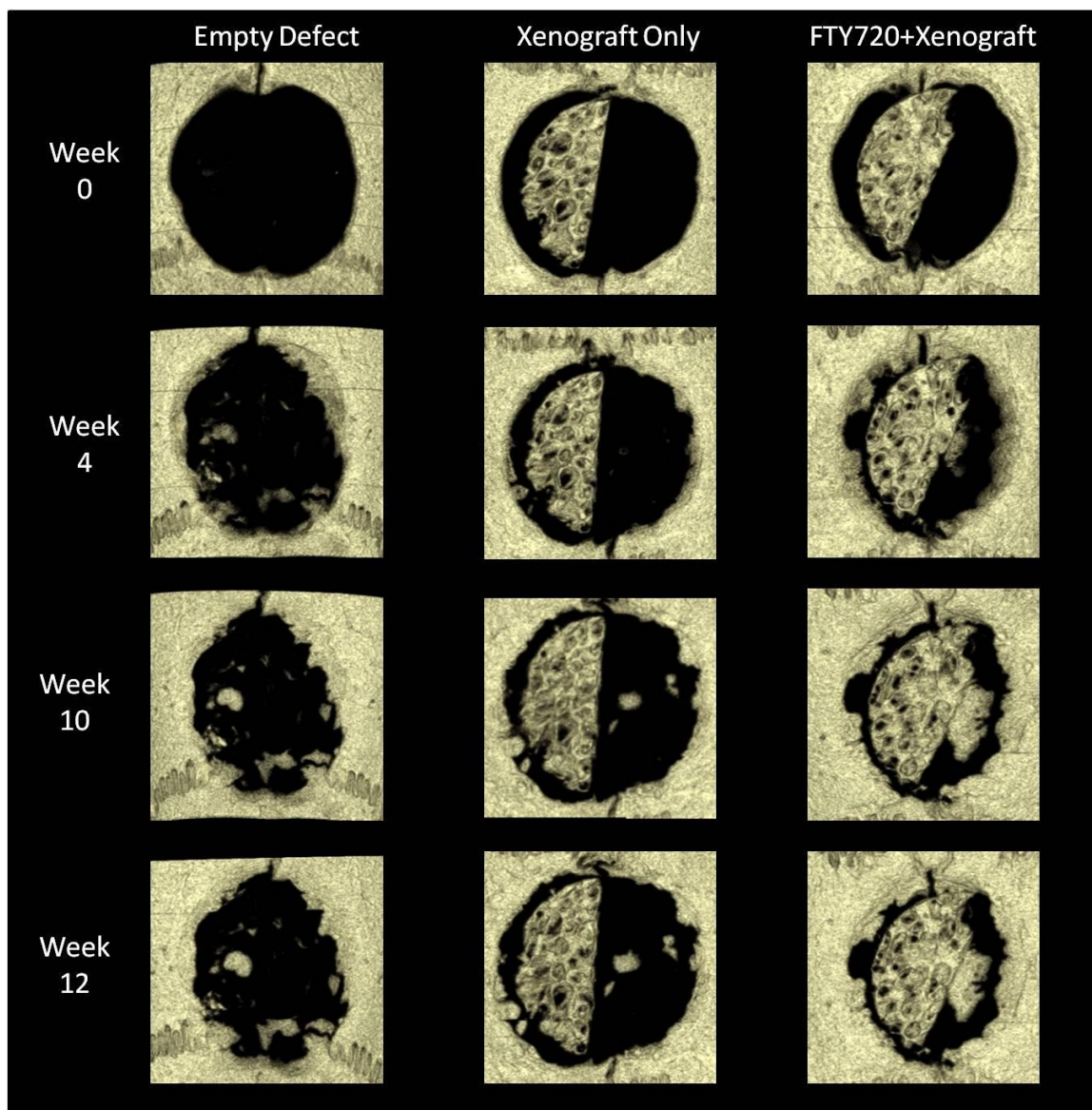


**Figure 11** Bone growth and xenograft remodeling in cranial defect area over 12 weeks. Representative *in vivo* MicroCT shows FTY720 adsorbed graft had improved bone growth in defect space similar to the result from the FTY720 loaded polymer coated allograft study. Empty defect showed random, undirected growth that began to regress after week 10.

Change in bone volume in the cranial defect area is shown in Figure 12 below for each time point. Differences at all time points were not statistically significant due to small animal numbers (n=3), but trends were observed. FTY720 accelerated bone growth in the area starting after week 2 above both controls. Empty defect had increased bone growth in earlier time points, but begins to regress after week 10 while FTY720 sustains and continues to improve bone growth.

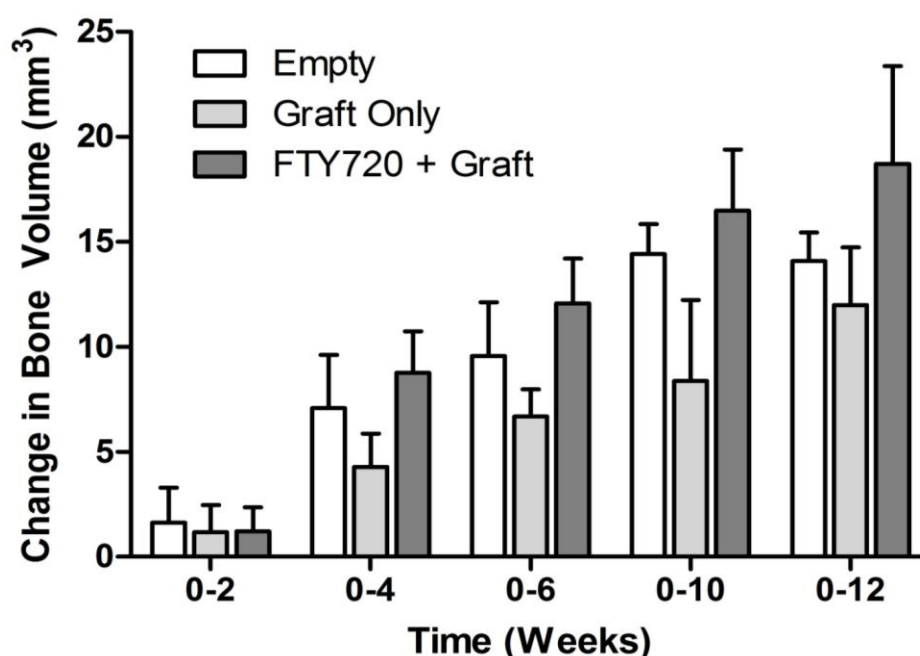


**Figure 12.** Change in bone volume in cranial defect area for empty, xenograft implanted, and FTY720 adsorbed xenograft over twelve weeks. FTY720 loaded xenograft spurred higher bone growth than xenograft alone after week two and sustained through week twelve. Empty defect bone growth lagged slightly behind the drug loaded group from week two and began to regress after week ten.

MicroCT visualization of cranial defect area's MICROFIL® perfused blood vessel network is shown below in Figure 13 with corresponding bone images. Blood vessels are shown in red, and soft tissue and demineralized bone are shown in tan. Empty defect clearly had more vessels and soft tissue in the defect space compared to the xenograft implanted groups. New bone growth in the FTY720 adsorbed xenograft

implanted defect seem accompanied by mature microvascular networks; particularly the void host edge and the void ingrowth from the graft had a growing network.

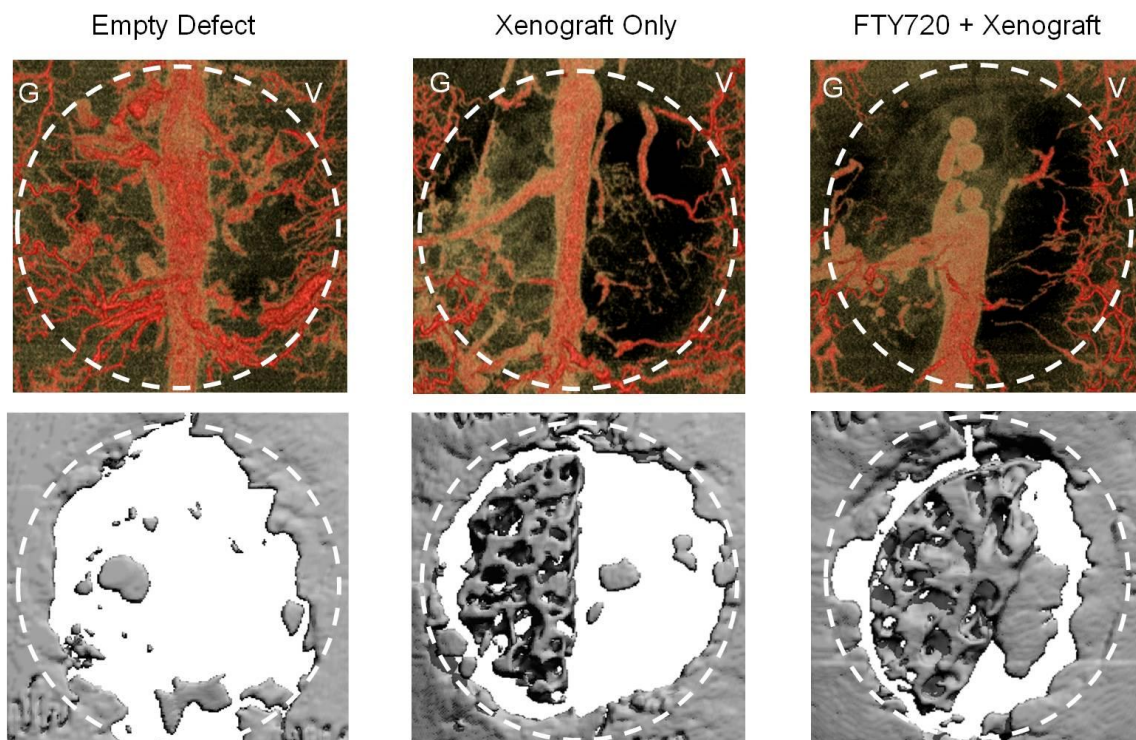


**Figure 13.** Blood vessel network in the calvarial defect area visualized by microCT of perfused MICROFIL® in top row, while bottom row shows corresponding bone in the area at week 12. Dotted circle approximates original defect, G is the graft side and V is the void side.

Blood vessel networks were quantified by whole defect area and as a ratio of graft side to void side vessels as shown in Figure 14 below. The sagittal sinus was intentionally excluded, and capillaries and small vessels were likely not well perfused, and thus not included in the calculations. Both empty defect and xenograft only groups had significantly higher blood vessel volumes than the FTY720 group. Xenograft only group had much lower graft to void side vessel volume ratio than the other groups.

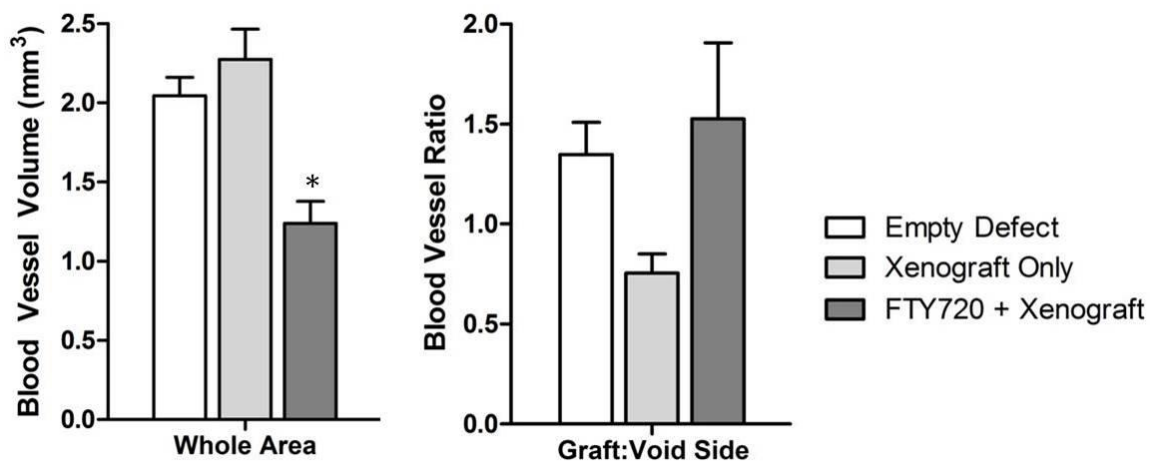


**Figure 14.** Blood vessel network volume was quantified at week 12 for the whole cranial defect area and a ratio of the graft side volume to void side volume. Empty defect and FTY720 xenografts saw approximately the same ratios while the xenograft had less vessel volume on the graft side compared to the void side. \*significant to other groups ( $p < 0.05$ ).

## Discussion

This work investigated the effects of local, sustained release of S1P receptor targeted drug FTY720 from cadaver bone grafts in critical size rat cranial defect model. S1P, a known immunomodulator, promotes lymphocyte egress (Schwab 2005; Pappu 2007) and induces an anti-inflammatory phenotype in macrophages (Hughes 2008); it also plays a role in regulating angiogenesis by inducing endothelial cell adherence junction assembly (Lee 1999), and endothelial cell migration (Lee 2001; Paik 2001) through S1P<sub>1</sub>. Several studies have established that S1P<sub>1</sub> also influences stem cell migration (Petrie Aronin 2010a; Ratajczak 2010). Thus, it is hypothesized that the mechanism by which FTY720, an S1P<sub>1</sub> agonist, accelerates bone formation is a combination of vascular remodeling, progenitor cell recruitment, and immunomodulation.

Delivery of FTY720 was initially achieved with continuous coating of PLAGA surrounding the bone implant. PLAGA has been extensively used for a variety of applications, such as bioactive molecule delivery (Langer 1993), guided bone regeneration (Oh 2006) and as a mechanically compatible scaffold for human trabecular bone applications (Saito 2010). Due to PLAGA's easily engineered properties, degradation and biocompatibility can be easily controlled for use in biological sites (Hasirci 2001; Reed 1981; Lu 1999) with minimal pH changes (Lu 1999), and it has been shown to be osteoconductive (Ishaug 1997). Though FTY720 encapsulation in a PLAGA scaffold allows for a slow sustained release while maintaining the porous structure of the scaffold (Petrie Aronin 2010a) and without disrupting osteoblast function during bone remodeling (Ishaug 1994), it might not last beyond a few weeks. Due to the high surface

area to volume ratio, low thickness, and 50% hydrophilic glycolic acid composition, the PLAGA coating is expected to completely degrade and release all FTY720 through bulk degradation within 4 to 8 weeks (Reed 1981; Lu 1999). Therefore, a more sustained and higher volume release system may be desirable for longer bone healing time frames such as long bone defects.

To this end, FTY720 was directly adsorbed to human bone xenografts in tenfold amounts in simpler and more translational loading method. Without having to consider disrupting the polymer coating, surgeons will be able to trim the bone graft to fit the defect space for better graft-host contact and union stability, which is vital to successful healing (Mankin 1987; Mankin 1996; Ortiz-Cruz 1997; Stevenson 1991). Also, by removing the polymer vehicle from the graft design, the therapy no longer must consider and avoid possible inhibitions to the regenerative process through unexpectedly harmful degradation products (Lieberman 2002).

The success of a graft implantation is measured by a combination of both new growth and graft integration. In order to quantify both these responses, semicircular grafts were used in the defects. Figure 4 shows that although initial bone growth is significant in the FTY720 groups compared to uncoated and coated controls, the total bone volume change is no longer significant at 8 weeks. Known patterns of PLAGA degradation and measurements of FTY720 release could potentially explain this effect. PLAGA degradation is characterized with an initial burst, as noted by 50% of the release occurring by day 5 and then a lag before the rate sharply increases again (Reed 1981; Lu 1999). Nevertheless, FTY720 does seem to accelerate this bone growth, as reflected in significantly high bone formation in the first few weeks. A study that evaluated the effect

of FDA approved alloplastic bone grafts in rat cranial defects found that treatment groups increased the rate of graft incorporation, and not total new bone formation (Mah 2004). Though the endpoint total bone volume growth in this study is not significantly increased by FTY720 groups, accelerating the rate of bone regeneration as observed in earlier weeks can have long term beneficial effects towards successful temporal evolution of bone growth. While the uncoated and coated groups exhibit undirected bone formation, it contributes to the total volume, and this contributes to the lack of significant total volume difference at week 8. Additionally, the inclusion of the sutured periosteum could have unexpectedly boosted bone growth in the uncoated and coated controls, due to the high level of osteoblast progenitor cells in the cambium layer (Augustin 2007) and defect protection (Lemperle 1998).

To assess the pattern of new bone formation and the quality of implant integration, evaluation included both the defect healing at the graft interface, and the new bone growth in the void region. Such qualitative evaluations have been utilized in previous studies to provide additional insights into the extent of bone regeneration initiated by different treatments (Johnson 1996; Patel 2008). Since the most significant growth was reflected at the end of 2 weeks, this method was applied both at that time point and at the end of the study. All groups demonstrate higher graft integration at week 8 compared to week 2, and the high loaded treatment group exhibits significantly (D) higher extensive graft directed growth after 8 weeks. It appears as though (C) initial acceleration of growth in the void as seen in the week 2 data translates into this extensive growth. As microvascular expansion is crucial for bone regeneration (Collin-Osdoby. 1994; Kleinheinz 2005; Murphy 2004), the earlier occurrence of a more developed

vasculature in the high loaded groups could potentially be the reason behind more extensive void region growth. Moreover, the assessment of bone formation in the void region indicates that the FTY720 loaded groups have a higher volume of directed growth towards the non-curved edge of the graft compared to the controls at both time points. The grafts are cut along the sagittal suture and have a dented edge that increases the surface area, causing a higher amount of drug-loaded polymer to accumulate in that region. It is hypothesized that this accumulation causes directed growth resulting in possible bridging. Histological examination of FTY720 loaded groups confirmed the qualitative analysis, as week 8 images showed mature bone growth incorporation with the graft and host bone; defect void space was well filled with mature bone formations and vascularized connective tissue.

Although FTY720 has proven efficacious in enhancing vascular growth and maturation in various animal models, its effects were mostly diminished by week 8 as there was no significant difference in the quantified blood vessel volume and vessel thickness as discerned by SMA staining (Figure 8 and 9). Previous work where FTY720 promoted arteriogenesis in the dorsal skinfold window chamber was not able to evaluate vascular remodeling beyond 3 weeks of drug application, due to model limitations (Sefcik 2011). Intramembranous bones are more challenging to vascularize than endochondral bones (Sullivan 1991), so FTY720's vascular effects may be more important in this study compared to an earlier study in tibial defects (Petrie Aronin 2010b). Patel released VEGF and BMP-2 individually and in combination in the cranial defect without significant effect on blood vessel volume at week 4 (Patel 2008). They concluded VEGF's influence may have been more notable at an earlier time point, or it

may have been too weak to sustain an enhanced, mature vasculature after 4 weeks. Indeed, it seems that week 8 was too late to capture differences due to FTY720 treatment in this study as well. However, the imaging method only allowed for visualization of vessels with a diameter larger than 20  $\mu\text{m}$ , precluding capillary and smaller blood vessel visibility. Therefore, FTY720 effects on microvasculature may have been missed due to imaging limitations. Additionally, the 3D vasculature images clearly show flat shapes that do not resemble vessels, due to MICROFIL® leakage from overly high perfusion pressure; these shapes were not included in the region of interest, but this may have introduced error into the blood vessel volume quantification (Bouxsein 2010).

FTY720 could also be aiding in recruiting circulating progenitor cells. In previous work, it was shown that S1P mediates dura stem cell migration in an S1P<sub>3</sub> dependent manner, as treatment with S1P increased their migration while treatment with VPC01091, a S1P<sub>3</sub> antagonist, did not (Petrie Aronin 2010a). High FTY720 loading in this study increased osteoclast precursor cell circulation (monocyte) levels significantly compared to other groups, although they still remained within the normal range (Figure 7). Perhaps through a related mechanism, S1P<sub>1</sub> agonism has been shown to affect osteoclastic activity in a post-menopausal osteoporotic mouse model, and the use of FTY720 resulted in decreasing the attachment of osteoclasts to the bone surface (Ishii 2009). It has also been established that FTY720 helps intestinal graft integration by preventing T cell infiltration (Kimura 2003). Both vascularization and progenitor cell recruitment are known to increase the rate of bone regeneration via graft integration and remodeling, and FTY720 is known to have an influence on both these processes. The increased acceleration of

bone regeneration observed at the end of week 2 could be attributed to a combination of these events.

### **Conclusion**

We have shown that FTY720 can be released in a local, sustained manner from cranial defect grafts for improved integration. Local drug delivery from coated grafts increased bone regeneration rate, graft integration, and directed bone growth in the void after 8 weeks of implantation in a critical size cranial defect. FTY720 loaded grafts had dose dependent effects, suggesting that drug encapsulation and release kinetics can be improved to obtain optimal bone growth profiles. Furthermore, bone xenografts currently being used in human patients can be loaded with FTY720 through direct adsorption with similar improved growth as in the polymer coated allografts; also, the drug release can be in higher quantities and for a longer time. Mechanisms for further exploration include early vascularization promotion, immune cell modulation, and osteoclast precursor cell circulation.

## References

- American Academy of Orthopaedic Surgeons (2011) Advisory Statement: Use of Musculoskeletal Tissue Allografts. Amer Academy of Orthopaedic
- Augustin G, Antabak A, Davila S (2007) The periosteum Part 1: Anatomy, histology and molecular biology. *Injury-Int J Care Inj* 38:1115-1130
- Bouxsein ML, Boyd SK, Christiansen BA, Guldberg RE, Jepsen KJ, Muller R (2010) Guidelines for assessment of bone microstructure in rodents using micro-computed tomography. *J Bone Miner Res* 25:1468-1486
- Boyce T, Edwards J, Scarborough N (1999) Graft bone. The influence of processing on safety and performance. *Orthop Clin North Am* 30:571-581
- Chen NT, Glowacki J, Bucky LP, Hong HZ, Kim WK, Yaremchuk MJ (1994) The roles of revascularization and resorption on endurance of craniofacial onlay bone grafts in the rabbit. *Plast Reconstr Surg* 93:714-724
- Collin-Osdoby P (1994) Role of vascular endothelial cells in bone biology. *J Cell Biochem* 55:304-309
- Cuvillier O, Pirianov G, Kleuser B, Vanek PG, Coso OA, Gutkind S, Spiegel S (1996) Suppression of ceramide-mediated programmed cell death by sphingosine-1-phosphate. *Nature* 381:800-803
- Delloye C, Cornu O, Druetz V, Barbier O (2007) Bone grafts: What they can offer and what they cannot. *J Bone Joint Surg Br* 89:574-579
- Delloye C, de Nayer P, Allington N, Munting E, Coutelier L, Vincent A (1988) Massive bone grafts in large skeletal defects after tumor surgery: a clinical and microradiographic evaluation. *Arch Orthop Trauma Surg* 107:31-41

- DePaula CA, Truncale KG, Gertzman AA, Sunwoo MH, Dunn MG (2005) Effects of hydrogen peroxide cleaning procedures on bone graft osteoinductivity and mechanical properties. *Cell Tissue Bank* 6:287-298
- Enneking WF and Campanacci DA (2001) Retrieved human grafts : a clinicopathological study. *J Bone Joint Surg Am* 83-A:971-986
- Friedlaender G, Mankin H, Goldberg V (2006) Bone Grafts and Bone Graft Substitutes. *Amer Academy of Orthopaedic* 1:90
- Giannoudis PV, Dinopoulos H, Tsiridis E (2005) Bone substitutes: An update. *Injury* 36:S20-S27
- Hasirci V, Lewandrowski K, Gresser JD, Wise DL, Trantolo DJ (2001) Versatility of biodegradable biopolymers: degradability and an in vivo application. *J Biotechnol* 86:135-150
- Huang CS, Das A, Barker DA, Tholpady SS, Wang TW, Cui Q, Botchwey EA. (2012) Local Delivery of FTY720 Accelerates Cranial Allograft Incorporation and Bone Formation. *Cell Tissue Res.* 347:553-566
- Hughes JE, Srinivasan S, Lynch KR, Proia RL, Ferdek P, Hedrick CC (2008) Sphingosine-1-phosphate induces an antiinflammatory phenotype in macrophages. *Circ Res* 102:950-958
- Ishaug SL, Crane GM, Miller MJ, Yasko AW, Yaszemski MJ, Mikos AG (1997) Bone formation by three-dimensional stromal osteoblast culture in biodegradable polymer scaffolds. *J Biomed Mater Res* 36:17-28
- Ishaug SL, Yaszemski MJ, Bizios R, Mikos AG (1994) Osteoblast function on synthetic biodegradable polymers *J Biomed Mater Res.* 28:1445-1453

- Ishii M, Egen JG, Klauschen F, Meier-Schellersheim M, Saeki Y, Vacher J, Proia RL, Germain RN (2009) Sphingosine-1-phosphate mobilizes osteoclast precursors and regulates bone homeostasis. *Nature* 458:524-528
- Johnson EE and Urist MR (2000) Human bone morphogenetic protein grafting for reconstruction of femoral nonunion. *Clin Orthop Relat Res* 371:61-74
- Johnson KD, Frierson KE, Keller TS, Cook C, Scheinberg R, Zerwekh J, Meyers L, Sciadini MF (1996) Porous ceramics as bone graft substitutes in long bone defects: A biomechanical, histological, and radiographic analysis. *J Orthop Res* 14:351-369
- Kimura T, Hasegawa T, Nakai H, Azuma T, Usui N, Sasaki T, Okada A (2003) FTY720 reduces T-cell recruitment into murine intestinal graft and prevents activation of graft-infiltrating cells. *Transplantation* 75:1469-1474
- Kleinheinz J, Stratmann U, Joos U, Wiesmann HP (2005) VEGF-activated angiogenesis during bone regeneration. *J Oral Maxillofac Surg* 63:1310-1316
- Langer R and Vacanti JP (1993) Tissue engineering. *Science* 260:920-926
- Lee MJ, Thangada S, Claffey KP, Ancellin N, Liu CH, Kluk M, Volpi M, Sha'afi RI, Hla T (1999) Vascular endothelial cell adherens junction assembly and morphogenesis induced by sphingosine-1-phosphate. *Cell* 99:301-312
- Lee MJ, Thangada S, Paik JH, Sapkota GP, Ancellin N, Chae SS, Wu M, Morales-Ruiz M, Sessa WC, Alessi DR, Hla T (2001) Akt-mediated phosphorylation of the G protein-coupled receptor EDG-1 is required for endothelial cell chemotaxis. *Mol Cell* 8:693-704

- Lemperle SM, Calhoun CJ, Curran RW, Holmes RE (1998) Bony healing of large cranial and mandibular defects protected from soft-tissue interposition: A comparative study of spontaneous bone regeneration, osteoconduction, and cancellous autografting in dogs. *Plast Reconstr Surg* 101:660-672
- Lieberman JR, Daluiski A, Einhorn TA (2002) The role of growth factors in the repair of bone. Biology and clinical applications. *J Bone Joint Surg Am.* 84-A:1032-1044
- Lu L and Mikos AG (1996) The importance of new processing techniques in tissue engineering. *MRS Bull* 21:28-32
- Lu L, Garcia CA, Mikos AG (1999) In vitro degradation of thin poly(DL-lactic-co-glycolic acid) films. *J Biomed Mater Res* 46:236-244
- Mah J, Hung J, Wang J, Salih E (2004) The efficacy of various alloplastic bone grafts on the healing of rat calvarial defects. *Eur J Orthod* 26:475-482
- Mankin HJ, Gebhardt MC, Tomford WW (1987) The use of frozen cadaveric allografts in the management of patients with bone tumors of the extremities. *Orthop.Clin.North Am.* 18:275-289
- Mankin HJ, Gebhardt MC, Jennings LC, Springfield DS, Tomford WW (1996) Long-term results of allograft replacement in the management of bone tumors. *Clin.Orthop.Relat.Res.* (324):86-97
- Mankin HJ, Hornicek FJ, Raskin KA (2005) Infection in massive bone grafts. *Clin Orthop Relat Res* 432:210-216
- Mokbel N, Bou Serhal C, Matni G, Naaman N (2008) Healing patterns of critical size bony defects in rat following bone graft. *Oral Maxillofac Surg* 12:73-78

- Murphy WL, Simmons CA, Kaigler D, Mooney DJ (2004) Bone regeneration via a mineral substrate and induced angiogenesis. *J Dent Res* 83:204-210
- Oh SH, Kim JH, Kim JM, Lee JH (2006) Asymmetrically porous PLGA/Pluronic F127 membrane for effective guided bone regeneration. *J Biomater Sci Polym Ed* 17:1375-1387
- Ortiz-Cruz E, Gebhardt MC, Jennings LC, Springfield DS, Mankin HJ (1997) The results of transplantation of intercalary allografts after resection of tumors. A long-term follow-up study. *J Bone Joint Surg. Am.* 79:97-106
- Paik J, During A, Harrison EH, Mendelsohn CL, Lai K, Blaner WS (2001) Expression and characterization of a murine enzyme able to cleave beta-carotene The formation of retinoids. *J Biol Chem* 276:32160-32168
- Pappu R, Schwab SR, Cornelissen I, Pereira JP, Regard JB, Xu Y, Camerer E, Zheng YW, Huang Y, Cyster JG, Coughlin SR (2007) Promotion of lymphocyte egress into blood and lymph by distinct sources of sphingosine-1-phosphate. *Science* 316:295-298
- Patel ZS, Young S, Tabata Y, Jansen JA, Wong ME, Mikos AG (2008) Dual delivery of an angiogenic and an osteogenic growth factor for bone regeneration in a critical size defect model. *Bone* 43:931-940
- Pebay A, Bonder CS, Pitson SM (2007) Stem cell regulation by lysophospholipids. *Prostaglandins Other Lipid Mediat* 84:83-97
- Petrie Aronin CE, Sefcik LS, Tholpady SS, Tholpady A, Sadik KW, Macdonald TL, Peirce SM, Wamhoff BR, Lynch KR, Ogle RC, Botchwey EA (2010a) FTY720

promotes local microvascular network formation and regeneration of cranial bone defects. *Tissue Eng Part A* 16:1801-1809

Petrie Aronin CE, Shin SJ, Naden KB, Rios PD, Jr, Sefcik LS, Zawodny SR, Bagayoko ND, Cui Q, Khan Y, Botchwey EA (2010b) The enhancement of bone graft incorporation by the local delivery of the sphingosine 1-phosphate receptor targeted drug FTY720. *Biomaterials* 31:6417-6424

Pinholt EM, Solheim E, Talsnes O, Larsen TB, Bang G, Kirkeby OJ (1994) Revascularization of calvarial, mandibular, tibial, and iliac bone grafts in rats. *Ann Plast Surg* 33:193-197

Ratajczak MZ, Lee H, Wysoczynski M, Wan W, Marlicz W, Laughlin MJ, Kucia M, Janowska-Wieczorek A, Ratajczak J (2010) Novel insight into stem cell mobilization-plasma sphingosine-1-phosphate is a major chemoattractant that directs the egress of hematopoietic stem progenitor cells from the bone marrow and its level in peripheral blood increases during mobilization due to activation of complement cascade/membrane attack complex. *Leukemia* 24:976-985

Reed AM and Gilding DK (1981) Biodegradable polymers for use in surgery — poly(glycolic)/poly(lactic acid) homo and copolymers: 2. In vitro degradation *Polymer* 22:494-498

Ryu J, Kim HJ, Chang EJ, Huang H, Banno Y, Kim HH (2006) Sphingosine 1-phosphate as a regulator of osteoclast differentiation and osteoclast-osteoblast coupling. *EMBO J* 25:5840-5851

Saito E, Kang H, Taboas JM, Diggs A, Flanagan CL, Hollister SJ (2010) Experimental and computational characterization of designed and fabricated 50:50 PLGA

porous scaffolds for human trabecular bone applications. *J Mater Sci Mater Med* 21:2371-2383

Schmitz JP and Hollinger JO (1986) The critical size defect as an experimental model for craniomandibulofacial nonunions. *Clin Orthop Relat Res* 205:299-308

Schwab SR, Pereira JP, Matloubian M, Xu Y, Huang Y, Cyster JG (2005) Lymphocyte sequestration through S1P lyase inhibition and disruption of S1P gradients. *Science* 309:1735-1739

Sefcik LS, Aronin CE, Awojodu AO, Shin SJ, Mac Gabhann F, MacDonald TL, Wamhoff BR, Lynch KR, Peirce SM, Botchwey EA (2011) Selective activation of sphingosine 1-phosphate receptors 1 and 3 promotes local microvascular network growth. *Tissue Eng Part A* 17:617-629

Sellers RS, Zhang R, Glasson SS, Kim HD, Peluso D, D'Augusta DA, Beckwith K, Morris EA (2000) Repair of articular cartilage defects one year after treatment with recombinant human bone morphogenetic protein-2 (rhBMP-2). *J Bone Joint Surg Am* 82:151-160

Sharma S, Mathur AG, Pradhan S, Singh DB, Gupta S (2011) Fingolimod (FTY720): First approves oral therapy for multiple sclerosis. *J Pharmacol Pharmacother* 2:49-51

Stevenson S, Li XQ, Martin B (1991) The fate of cancellous and cortical bone after transplantation of fresh and frozen tissue-antigen-matched and mismatched osteochondral allografts in dogs. *J Bone Joint Surg Am.* 73:1143-1156

Stevenson S, Emery SE, Goldberg VM (1996) Factors affecting bone graft incorporation. *Clin Orthop Relat Res* 324:66-74

- Sullivan WG and Szwajkun PR (1991) Revascularization of cranial versus iliac crest bone grafts in the rat. *Plast Reconstr Surg* 87:1105-1109
- Thompson RC, Jr, Pickvance EA, Garry D (1993) Fractures in large-segment grafts. *J Bone Joint Surg Am* 75:1663-1673
- Wheeler DL and Enneking WF (2005) Graft bone decreases in strength in vivo over time. *Clin Orthop Relat Res* 435:36-42
- Yazici C, Takahata M, Reynolds DG, Xie C, Samulski RJ, Samulski J, Beecham EJ, Gertzman AA, Spilker M, Zhang X, O'Keefe RJ, Awad HA, Schwarz EM (2011) Self-complementary AAV2 5-BMP2-coated Femoral Grafts Mediated Superior Bone Healing Versus Live Autografts in Mice With Equivalent Biomechanics to Unfractured Femur. *Mol Ther* [Epub ahead of print]
- Younger EM and Chapman MW (1989) Morbidity at bone graft donor sites. *J.Orthop.Trauma* 3:192-195
- Zhang H, Desai NN, Olivera A, Seki T, Brooker G, Spiegel S (1991) Sphingosine-1-phosphate, a novel lipid, involved in cellular proliferation. *J Cell Biol* 114:155-167